Sensors and Actuators A 166 (2011) 66–77

Contents lists available at ScienceDirect

Sensors and Actuators A: Physical

journal homepage: www.elsevier.com/locate/sna

Motion behavior of triangular waveform excitation input in an operating impact drive mechanism

Chia-Feng Yang[a], Shyr-Long Jeng[b], Wei-Hua Chieng[a,*]

[a] Department of Mechanical Engineering, National Chiao Tung University, 1001 University Road, Hsinchu City 300, Taiwan, ROC
[b] Department of Automatic Engineering, Ta Hwa Institute of Technology, No. 1, Dahua Road, Qionglin Shiang Hsinchu County 307, Taiwan, ROC

ARTICLE INFO

Article history:
Received 15 June 2010
Received in revised form
10 December 2010
Accepted 10 December 2010
Available online 23 December 2010

Keywords:
Impact drive mechanism (IDM)
Stepping motion
Step size
Motion behavior
Piezoelectric actuator

ABSTRACT

Stable stepping motion from mechanical excitation of a piezoelectric device is generated using the impact drive mechanism (IDM) based on various triangular waveforms exerted by the counter mass speed. However, stick-slip behavior originating from the contact friction between the movable part and the guide surface poses an obstacle for precise modeling. Therefore, this work presents a concise impulse model for mechanism control of stepping motion behavior. The proposed impulse model incorporates the duty ratio and input frequency of the triangular waveform of counter mass relative displacement as the system input and outputs the estimated step size and the behavior of the stepping motion. An enhanced version of the dynamic model and our experimental results validate the efficacy of the proposed model. An adequate design and control of IDM motion is highly promising for use in nano-scale positioning.

1. Introduction

Among the many piezoelectric precision positioning systems developed for industrial and scientific applications include scanning displacement devices, pulse drive devices and ultrasonic piezomotors [1]. Scanning displacement devices produce motion that is driven directly or mechanically amplified. Pulse drive devices based on the inertial principle include stick-slip and other clamping mechanisms. A stick-slip mechanism based on the rapid response of continuous driving voltage can generate stable stepping motion from mechanical excitation of a piezoelectric device. Stick-slip behavior results from the contact friction between a movable part and a guided surface. Despite the apparent ability of a pulse drive device to resolve the limited stroke problem of a scanning device, some bottlenecks remain, including low load capacity of a pulse drive device. Load variation significantly alters the mechanism behavior. The stick-slip motion is sensitive to changes in nearby surroundings, such as the indeterminate distribution of friction on the guided surface, tilting of the guide surface and mechanical vibration. These quasi-static piezoelectric motors are distinct significantly differ from ultrasonic piezomotors. Ultrasonic piezomotors convert electro-mechanical energy on piezoelectric components that transport an acoustic standing wave or traveling wave (surfing wave) smoothly [2,3]. An acoustic wave produced by resonantly excited piezoelectric materials induces the mechanical movement for rotating or sliding motion.

IDMs have been applied include its use as a rotating joint within a micro robot arm [4], not only as an actuator for positioning printed circuit boards [5], but also as a movable platform to machine fine structures on a large work piece [6]. Driving IDM should consider the particular waveform of an input signal amplified to a high voltage [7,8]. Ha et al. [9] attempted to optimize an excitation waveform for driving IDM with a real-coded genetic algorithm and, in doing so, achieved the farthest step size under the same conditions of amplitude and frequency of input signal. In some applications suffering from an adverse environment, a non-contact method of thermally exciting the actuators of IDM has been developed [10,11]. For the precision positioning motion of IDM, a previous study integrated the Leuven model for the frictional force and the Bounc–Wen model for the hysteresis effects with the distributed parameter system and formulated using the finite-element method (FEM) [12]. Other applications involving positioning devices with IDM have also been developed for new materials driven by a magnetic force [13–15]. Impressively, the demonstrations promulgate a 10 nm high precision step size through means of two-stage control strategies and a combination of piezo-VCM (voice-coil motors) actuators or piezo-pneumatic actuators with an adjusting preload mechanism in Refs. [16,17].

A mathematical model of a spring–damper–mass system for a linear motor using the IDM has been devised [18,19]. The subse-

* Corresponding author. Tel.: +886 3 571 2121x55152; fax: +886 3 572 0634.
E-mail address: whc@cc.nctu.edu.tw (W.-H. Chieng).

0924-4247/$ – see front matter © 2010 Elsevier B.V. All rights reserved.
doi:10.1016/j.sna.2010.12.008

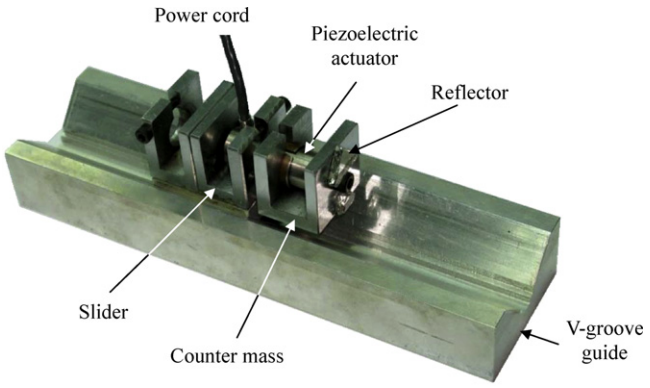

Fig. 1. The Impulse Drive Mechanism (IDM).

quent dynamic behavior of an IDM system influences the driving input voltage and waveform frequency. For reason of optimizing moving behavior of IDM, various waveforms [19] of driving IDM are discovered according to this dynamic model. In fact, since that nonlinearity of the hysteresis and friction [20] results in the inaccuracy of dynamic model and the consequence of control strategy [21], the phenomenon comes into existence of different motion behaviors exciting by triangular waveform in experiments. This work proposes a concise impulse model to describe stepping motion behaviors of IDM and indicates not all inputs of the duty and frequency of triangular waveform work as well. In the experiments, this work selects the piezoelectric material-based IDM as the precise positioning for the proposed impulse model. The following sections describe the stepping behavior of IDM.

2. Impulse model of IDM

IDM consists of the main mass, a piezoelectric actuator and a counter mass. A slider may be mounted on a V-groove guide way and held steadily by the friction force when no input voltage is applied to the piezoelectric actuator, as shown in Fig. 1. The V-groove guide can produce a one-dimensional motion constraint and provide a necessary alignment for laser interferometer measurement simultaneously. A counter mass is connected to the main object via one piezoelectric element. The mechanism performs the stepping motion and elongating or contracting the piezoelectric actuator by applying voltage waveforms to the piezoelectric actuator, as found in literature [5,6,11,12,16].

Fig. 2 shows a simplified IDM model and its block diagram. The variables X and x denote the displacement of the slider, as well as the relative displacement between the counter mass and slider, respectively. Whenever the time derivative of the stroke, $\dot{x}(t)$, is discontinuous at time t, an impulse motion occurs at both the slider and the counter mass. The equations can thus be used as followings:

$$\dot{X}(t) = \dot{X}(t_-) + \frac{P}{M} \tag{1}$$

and

$$\dot{x}(t) = \dot{x}(t_-) - \frac{M+m}{Mm}P \tag{2}$$

where t_- denotes the time with an infinitesimally small time interval ahead of t. M and m denote the mass of the slider and the counter mass, respectively. The piezoelectric actuator mass could be included in M or neglected since the housing type of piezoelectric materials. The amount of impulse (momentum) P can be evaluated according to

$$P = \frac{Mm}{M+m}(\dot{x}(t_-) - \dot{x}(t)) \tag{3}$$

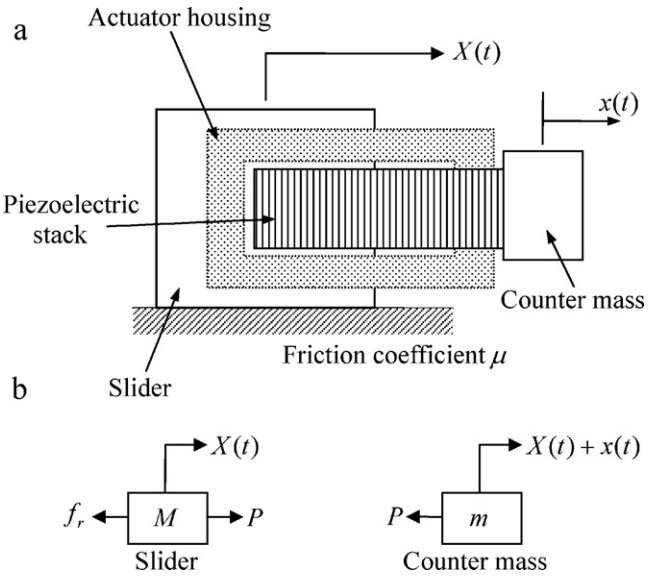

Fig. 2. (a) Schematic of impulse model of IDM. (b) Block diagram of impulse model.

2.1. Impulse motion due to triangular waveform excitation

According to Fig. 3, the triangular wave form input to the piezoelectric actuator can be written as follows:

$$\dot{x}(kT+t) = \begin{cases} 0 & k < 0 \\ \dfrac{S}{\gamma T} & \text{when} \quad 0 \le t < \gamma T \\ \dfrac{-S}{(1-\gamma)T} & \gamma T \le t < T \end{cases} \tag{4}$$

where S denotes the maximum displacement of the piezoelectric actuator, γ denotes the duty ratio of the triangular wave and $0 < \gamma < 1$. Two phases, i.e. the extension and retraction phases, are applied alternatively to the piezoelectric actuator which is used to connect the slider and counter mass. Between the phases, the impulse is introduced to cause velocity discontinuity of both the slider and counter mass. Switching from the retraction phase to the extension phase is considered first. Substituting $t = kT$ with Eq. (3) yields

$$P_1 = \frac{Mm}{M+m}(\dot{x}(kT_-) - \dot{x}(kT)) = \frac{Mm}{M+m}\left(\dot{x}(kT_-) - \frac{S}{\gamma T}\right) \tag{5}$$

where P_1 denotes the corresponding impulse produced by piezoelectric actuator input at this instant. Rewriting Eq. (1) by substituting Eq. (5) follows

$$\dot{X}(kT) = \dot{X}(kT_-) + \frac{m}{M+m}\left(\dot{x}(kT_-) - \frac{S}{\gamma T}\right) \tag{6}$$

as the points A and B shown in Fig. 3. During the extension phase, the friction force is introduced to prevent the slider from sliding relative to the ground as following

$$\dot{X}(kT+t) = \dot{X}(kT_-) + \frac{m}{M+m}\left(\dot{x}(kT_-) - \frac{S}{\gamma T}\right) + \mu g t \tag{7}$$

where the friction coefficient μ is chosen to be positive for $\dot{X}(kT+t) < 0$. The slider may come to a full stop when the impulse P_1 cannot keep the slider from moving during the entire extension phase. As the point C shown in Fig. 3, the solution at the end of the extension phase may be

$$\dot{X}(kT+\gamma T_-) = \dot{X}(kT_-) + \frac{m}{M+m}\left(\dot{x}(kT_-) - \frac{S}{\gamma T}\right) + \mu g T\gamma < 0 \tag{8a}$$

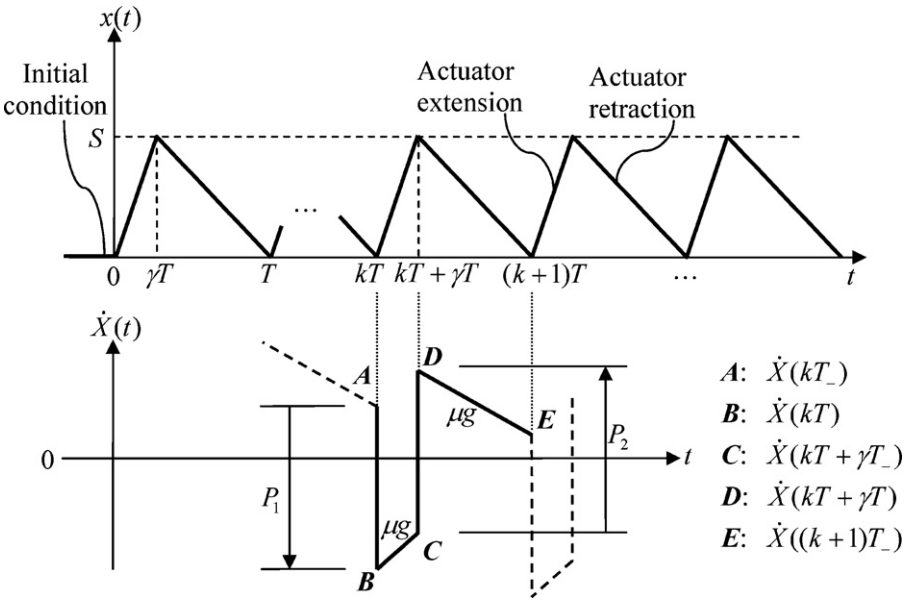

Fig. 3. The input triangular waveform $x(t)$ for piezoelectric actuator and the induced slider velocity $\dot{X}(t)$ of IDM.

or

$$\dot{X}(kT+\gamma T_{-})=0 \tag{8b}$$

Next, switching from the extension phase to the retraction phase is considered. Similarly, by substituting $t=(k+\gamma)T$ with Eq. (3), the following relation from Eq. (4) is obtained

$$P_2=\frac{Mm}{M+m}(\dot{x}(kT+\gamma T_{-})-\dot{x}(kT+\gamma T))=\frac{Mm}{M+m}\left(\frac{S}{(1-\gamma)\gamma T}\right) \tag{9}$$

where P_2 denotes the corresponding impulse produced by piezoelectric actuator input. By substituting Eq. (9) with Eq. (1) yields the following:

$$\dot{X}(kT+\gamma T)=\dot{X}(kT+\gamma T_{-})+\frac{m}{M+m}\left(\frac{S}{(1-\gamma)\gamma T}\right) \tag{10}$$

During the retraction phase as shown the region between the points D and E in Fig. 3, the friction force is introduced to prevent the slider from sliding relative to the ground so that

$$\dot{X}(kT+t)=\dot{X}(kT+\gamma T)-\mu g(t-\gamma T) \tag{11}$$

where the friction coefficient μ is chosen to be positive for $\gamma T\le t<T$. Rearranging Eqs. (8a), (10) and (11) yields

$$\dot{X}(kT+t)=\dot{X}(kT_{-})+\frac{m}{M+m}\left(\dot{x}(kT_{-})+\frac{S}{(1-\gamma)T}\right)+\mu g(2\gamma T-t) \tag{12a}$$

for $\gamma T\le t<T$. Also, rearranging Eqs. (8b), (10) and (11) yields

$$\dot{X}(kT+t)=\frac{m}{M+m}\left(\frac{S}{(1-\gamma)\gamma T}\right)-\mu g(t-\gamma T) \tag{12b}$$

for $\gamma T\le t<T$. The slider may come to a full stop when the impulse P_2 cannot keep the slider from moving during the entire retraction phase, i.e.

$$\dot{X}((k+1)T_{-})=0 \tag{12c}$$

2.2. Steady state analysis

Subjected to one-sided (towards the slider) movement control, the duty ratio must be less than 50%, i.e. $\gamma<0.5$. The triangular waveform exciting on the piezoelectric actuator is repetitive according to Eq. (4) for $k>0$. The situation of steady state shows the initial condition of piezoelectric actuator velocity before each cycle is

$$\dot{x}(kT_{-})=-\frac{S}{(1-\gamma)T} \tag{13}$$

Note that the periodic triangular waveform schemes the mirror transition corners, the momentum P_1 and P_2 are equal but opposite except for $k=0$. Substituting Eq. (13) with Eq. (12a) yields

$$\dot{X}(kT+t)=\dot{X}(kT_{-})-\mu g(t-2T\gamma)>0 \tag{14}$$

for $\gamma T\le t<T$. The condition for a slider to come to a full stop before the end of the retraction phase, i.e. $\dot{X}(NT_{-})=0$, for certain $k=N$ is

$$\mu gT(1-2\gamma)\ge\dot{X}((N-1)T_{-})>0 \tag{15}$$

According to Eqs. (14) and (15), once the slider stopped in the retraction phase, it must consequently come to a full stop before the end of retraction phase for all $k\ge N$ to achieve a steady state, i.e.

$$\dot{X}(kT_{-})=0 \quad \text{for} \quad k\ge N \tag{16}$$

The precondition for validity of Eq. (12a) is that Eq. (8a) must not be zero at all instances in the interval $0\le t<\gamma T$. Thus, when a steady state is achieved, Eqs. (13) and (16) can be substituted with Eq. (8a) to obtain that

$$\frac{m}{M+m}\left(\frac{S}{(1-\gamma)\gamma T}\right)>\mu gT\gamma \tag{17}$$

Let the impulse ratio η be defined as

$$\eta=\frac{mS}{(M+m)\mu gT^2} \tag{18}$$

and then Eq. (17) yields the following:

$$\eta>(1-\gamma)\gamma^2 \tag{19}$$

In case that Eq. (19) is valid, velocity of the IDM is determined using the following velocity equation

$$\dot{X}(nT+t)=\begin{cases}\mu gt-\dfrac{m}{M+m}\left(\dfrac{S}{(1-\gamma)\gamma T}\right) & 0\le t<\gamma T\\ \mu g(2T\gamma-t) & \gamma T\le t<2\gamma T\end{cases} \quad \text{when} \tag{20}$$

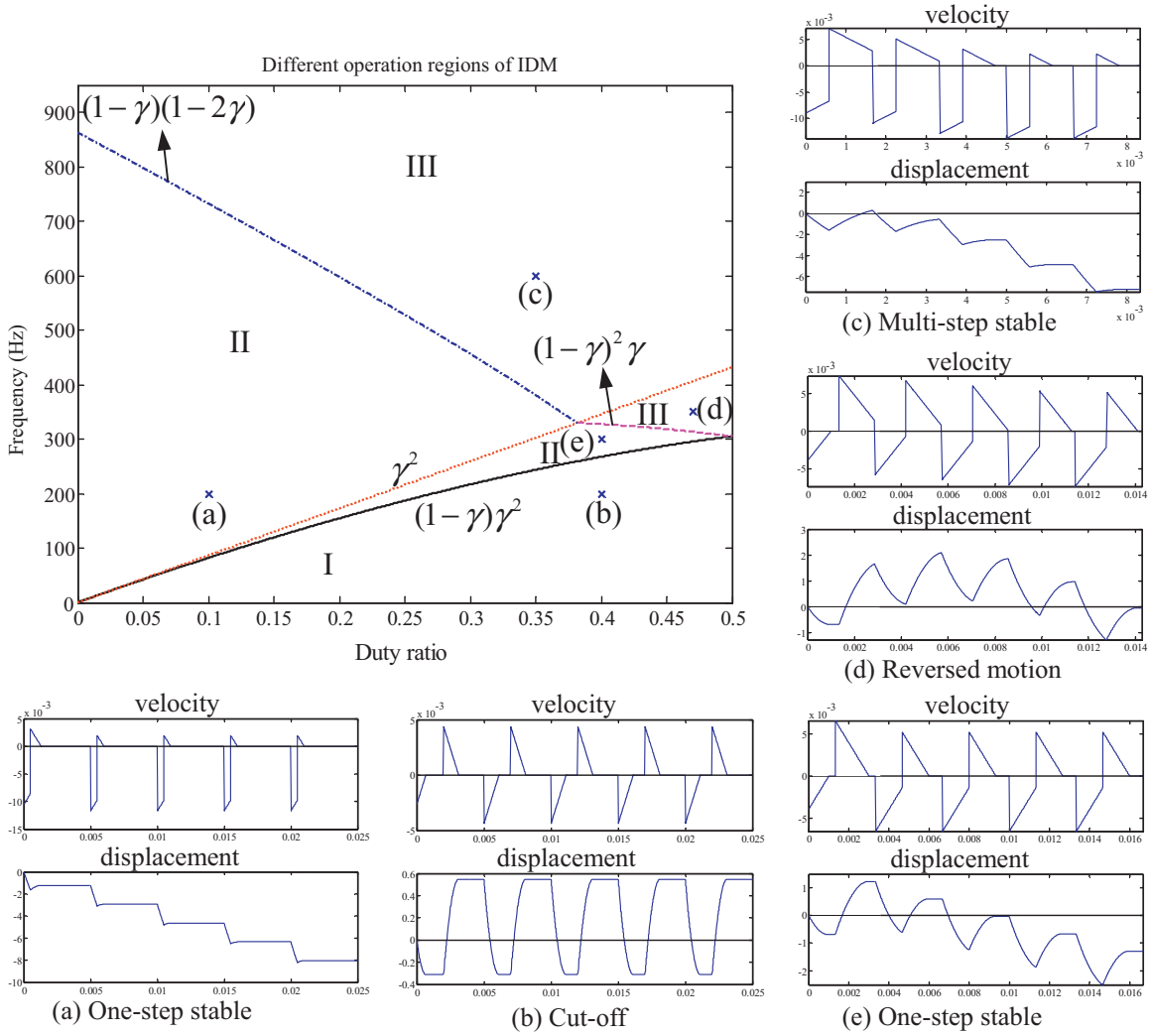

Fig. 4. Different regions for estimating stepping-motion behavior of IDM with parameters (a) $(\gamma, f) = (0.1, 200)$ and $\eta = 0.054$; (b) $(\gamma, f) = (0.4, 200)$ and $\eta = 0.054$; (c) $(\gamma, f) = (0.35, 600)$ and $\eta = 0.482$; (d) $(\gamma, f) = (0.47, 350)$ and $\eta = 0.164$; (e) $(\gamma, f) = (0.4, 300)$ and $\eta = 0.121$.

when the steady state is achieved. The step size of the IDM motion can be derived by integrating Eq. (20) with the initial condition $\dot{X}(NT_-) = 0$ as following:

$$\begin{aligned}\Delta X(NT) &= X((N+1)T) - X(NT) \\ &= -\left(\frac{m}{(M+m)(1-\gamma)}S - \mu g\gamma^2 T^2\right)\end{aligned} \tag{21}$$

According to [17], adding a preload force on the slider is equivalent to increasing frictional coefficients μ in both static and kinetic regions. The step size may be refined by either properly adjusting μ, or adjusting the preload, to match the slider displacement induced by S (the maximum displacement of the piezoelectric actuator). In the extreme case that $\mu \to (m/(g\gamma^2 T^2(M+m)(1-\gamma)))S$, the step size approaches theoretically, according to Eq. (21), to zero or an infinitely small size. The consequence of a miniature step size may be useful in the applications involving advanced measurement schemes for nano-scale positioning.

However, the practical piezoelectric actuator cannot produce velocity discontinuity, implying that an infinite acceleration is required. The above equation for step size estimation can thus be attenuated as follows:

$$\begin{aligned}\Delta X &= \alpha\left(\mu g\gamma^2 T^2 - \frac{m}{(M+m)(1-\gamma)}S\right) \\ &= \alpha\left(\gamma^2 - \frac{\eta}{(1-\gamma)}\right)\mu g T^2\end{aligned} \tag{22}$$

where α refers to the correction factor and $0 < \alpha < 1$.

The precondition for the validity of Eq. (12b) is Eq. (8b) during the interval $0 \le t < \gamma T$, that implies

$$\eta \le (1-\gamma)\gamma^2 \tag{23}$$

The corresponding step size may be derived by integrating Eqs. (7) and (12b) with the initial condition $\dot{X}(NT_-) = 0$ as that

$$\Delta X(NT) = X((N+1)T) - X(NT) = 0 \tag{24}$$

Eq. (24) implies that although the steady state can be achieved when Eq. (21) is violated, however, the slider will have no net displacement in whole. The fateful behavior of movement is determined by either Eq. (19) or Eq. (23) as IDM achieves a steady state. Fig. 4(a) shows the response of a simulation for $\eta \le (1-\gamma)\gamma^2$ with system parameters listed in Table 1.

Table 1
System parameters of the IDM used in the simulations and experiments.

Symbol	Physical meaning	Quantity
M	Mass of slider	165.57 g
m	Mass of counter mass	57.61 g
μ	Friction coefficient	0.4
g	Acceleration of gravity	9.8 m/s^2
S	Stroke of piezoelectric actuator	20.35 μm
α	Step size correction factor	0.35

2.3. Transient analysis

Transient response attributed to the initial condition of the piezoelectric actuator differs from the consecutive periodic triangular waveform. Transient response should be as short as possible to achieve highly accurate position control. At the initial time $k=0$, we have $\dot{X}(0_-)=0$ and $\dot{x}(0_-)=0$. Additionally, Eq. (7) indicates that the slider velocity is obtained during the extension phase, $0 \le t < \gamma T$, so that

$$\dot{X}(\gamma T_-) = \begin{cases} \mu g \gamma T - \dfrac{m}{M+m}\left(\dfrac{S}{\gamma T}\right) & \text{if } \eta > \gamma^2 \\ 0 & \text{if } \eta \le \gamma^2 \end{cases} \tag{25}$$

In a case in which $\eta > \gamma^2$, the terminal velocity at the end of the first step is derived from Eq. (12a) for $\gamma T \le t < T$ as follows:

$$\dot{X}(T_-) = \begin{cases} \left(\dfrac{\eta}{(1-\gamma)} - (1-2\gamma)\right)\mu g T & \text{if } \eta > (1-\gamma)(1-2\gamma) \\ 0 & \text{if } \eta \le (1-\gamma)(1-2\gamma) \end{cases} \tag{26}$$

In another case in which $\eta \le \gamma^2$, the terminal velocity at the end of the first step is derived from Eq. (12b) for $\gamma T \le t < T$ as follows:

$$\dot{X}(T_-) = \begin{cases} \left(\dfrac{\eta}{(1-\gamma)\gamma} - (1-\gamma)\right)\mu g T & \text{if } \eta > (1-\gamma)^2\gamma \\ 0 & \text{if } \eta \le (1-\gamma)^2\gamma \end{cases} \tag{27}$$

The steady-state condition is achieved after the first step, i.e. $N=1$, when $\dot{X}(T_-)=0$. Based on the steady state analysis, the slider's terminal velocity of the first triangular waveform input discriminates whether the following steps are identical or not. Not until the slider is caught in a stop does the contact friction force act persistently upon it. For the slider containing velocity at the first terminal, additional steps must be taken to achieve the steady state within a finite time. The impulse model also explains the transient response accompanied by a reverse movement within the first few steps occasionally. High accuracy of position control is generally accomplished within the first few steps and, hence, reverse versions are not anticipated.

Steady-state and transient response analyses indicate that four boundaries, i.e. $(1-\gamma)\gamma^2$, γ^2, $(1-\gamma)(1-2\gamma)$ and $(1-\gamma)^2\gamma$, locate the operating region of IDM with the switching frequency defined as $f=1/T$. Fig. 4(a)–(e) schematically depicts the transient response of an impulse model for different operation regions, with the system parameters listed in Table 1.

As has been explained, three behavioral regions of operating IDM with the triangular waveform excitation input (Fig. 4), referred to as stepping motion behavior for operating IDM, are defined as

1. *Cut-off region*: When $\eta \le (1-\gamma)\gamma^2$, the steady-state impulse induced from extension and retraction of the piezoelectric actuator cannot sufficiently yield a movement for IDM, as shown in region I of Fig. 4(b).
2. *One-step stable region*: When the motion of IDM falling into standstill during extraction phase of the first step, the steady-state impulse subsequently induced from the extension and retraction of the piezoelectric actuator can not sufficiently yield a movement for IDM, as shown in region II of Fig. 4(a) and (e). For applications requiring high precision incremental positioning, e.g., incremental positioning precision is less than 1 μm, the incremental movement must be achieved exactly in the initial steps. In the one-step stable region, the impulse ratio η satisfies the following set:

$$\{\eta | \eta > (1-\gamma)\gamma^2, \eta < (1-\gamma)^2\gamma\} \cup \{\eta | \eta > \gamma^2, \eta < (1-\gamma)(1-2\gamma)\} \quad \text{for} \quad 0 < \gamma < 0.5 \tag{28}$$

3. *Multi-step stable region*: When velocity occurs at the end of the first step, the steady-state impulse induced from the extension and retraction of the piezoelectric actuator can sufficiently yield a movement for the IDM. However, the initial impulse is too large to cause the initial step of the motion not falling into the steady state, as shown in region III of Fig. 4(c) and (d). In the multi-step stable region, the impulse ratio η satisfies the following set:

$$\{\eta | \eta > (1-\gamma)(1-2\gamma), \eta > (1-\gamma)^2\gamma\} \quad \text{for} \quad 0 < \gamma < 0.5 \tag{29}$$

Table 2
The specifications of Burleigh's piezoelectric actuator.

Specifications	Description
Model number	PZL-015
Materials	Lead zirconate titanate (PZT)
Type	Preloaded stack actuator with housing
Dimension	Piezo stack: rectangular disk 4 mm × 5 mm 0.25 mm thickness PZT plate Total stack length: 20 mm Housing: diameter 12.7 mm, length 33.8 mm
Operating voltage	−20 to 150 V
Motion for 0–100 V	−5 to 23 μm
Frequency response	3.5 kHz
Nonlinearity	4%
Hysteresis	15%
Creep	Increasing voltage: 1–2% in 20–30 s Decreasing voltage: 7–8% in 60–80 s

3. Experiments

In the experiment, the excitation triangular waveform is formed using NI DAQ-card PCI-6711 which features a 12-bit digital-to-analog converter (DAC) per channel. The signal is controlled by a LabVIEW software, amplified maximal to 130V by Burleigh PZ-350M Amplifier, and then fed into piezoelectric actuator of IDM on the V-groove guide way. Fig. 5 illustrates the overall system architecture and configuration with instrumentation for evaluating the displacement of the piezoelectric actuator. The HP10705A single beam interferometer with 10 nm (0.4 μin.) resolution and 3 MHz maximum data update rate determines the displacement of IDM. The sampling time of the data is controlled by the DSP module and, then, sent to HP10885A axis board in PC. The HP10885A axis board focuses mainly on converting the reference and measured signals from a HP5517C interferometer laser head and measurement receiver into a 32-bit digital position word. The unit of measurement associated with the position word is a fraction of the wavelength of the laser light currently used. Following conversion, the raw data is read by the DSP module directly. The DSP module focuses mainly on sending signals to HP10885A axis board to control the sequence of data sample and hold (8 bits digital output) and performing data reading (32 bits digital input). These objectives are achieved by integrating these tasks into a program that can be loaded to the DSP controller through use of developmental software. Table 2 lists the specifications of the piezoelectric actuator that is applied in the experiments (Fig. 6).

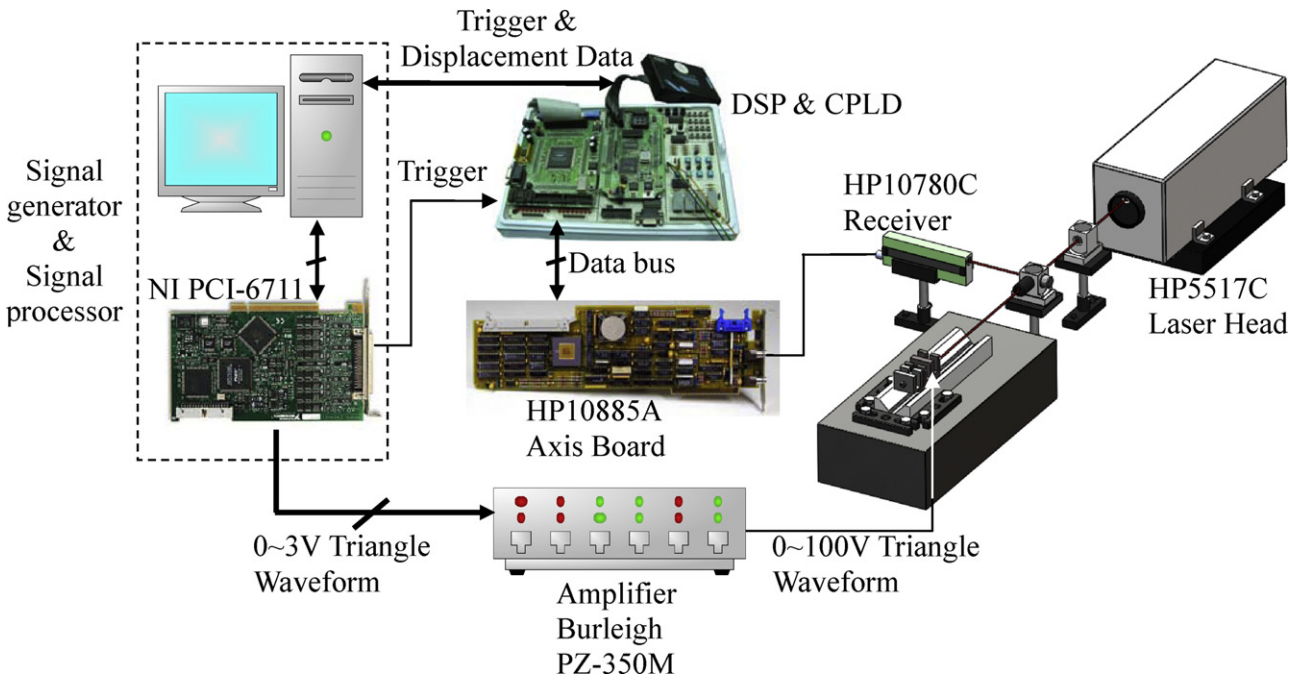

Fig. 5. The architecture of stepping motion experiments using IDM.

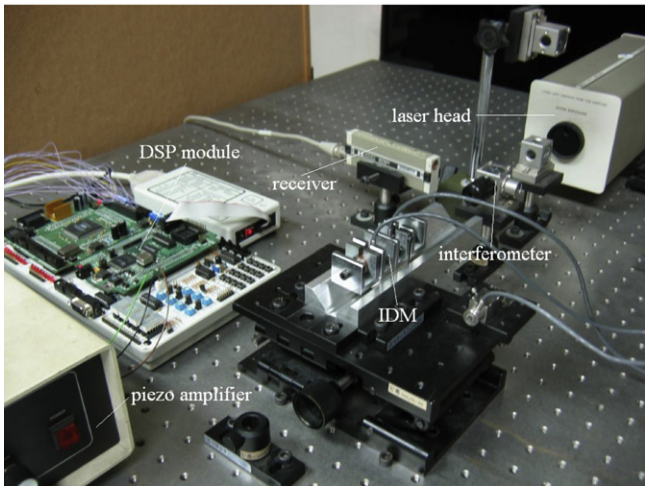

Fig. 6. Experimental setup for evaluating stepping motion of IDM.

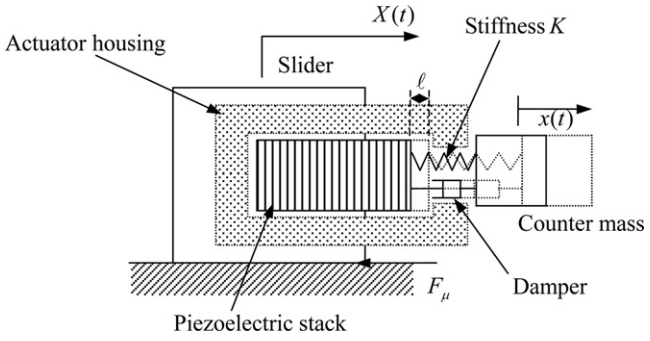

Fig. 7. Schematic of mass–damper–spring dynamic model of IDM.

4. Mass–damper–spring dynamic model

In the foregoing section, an impulse model has been developed for predicting the behavior of IDM motion. The impulse model is simplified dynamic model without considering the detail spring and damper effect of the IDM. Through the impulse model analysis, it is convenient to obtain the one-step stability of the IDM motion. However, the corresponding transient response is inaccurate as a result of the simplified model. On the other hand, a better precise dynamic analysis, referred the mass–damper–spring dynamic model [19,20,22,23], may be used to analyze the spring–damper effect during each impulse step. The coefficients of the mass–damper–spring dynamic model are obtained from experiments based on the known system identification techniques. The mass–damper–spring model of IDM as shown in Fig. 7 is expressed as follows:

$$\begin{cases} M\ddot{X} - C\dot{x} - Kx = F_\mu - (C\dot{\ell} + K\ell) \\ m(\ddot{X} + \ddot{x}) + C\dot{x} + Kx = C\dot{\ell} + K\ell \end{cases} \tag{30}$$

where ℓ and F_μ denote the piezoelectric actuator length input and the frictional force between the two surfaces in contact, respectively. Friction force F_μ is evaluated by the stick-slip friction model [24–27] based on the relative velocity $\dot{X}$ between these two contacting surfaces.

The housing piezoelectric actuator is assumed here to be linear and rigid. According to the piezoelectric actuator design, the mechanical interface between the slider and the counter mass is specified as a linear spring constant K and a linear damping coefficient C. While assuming that no contact friction occurs between the counter mass and the guide way, friction occurs only between the slider and the guide way. The variables X and x refer to the displacement of the slider, as well as the relative displacement between the counter mass and slider, respectively.

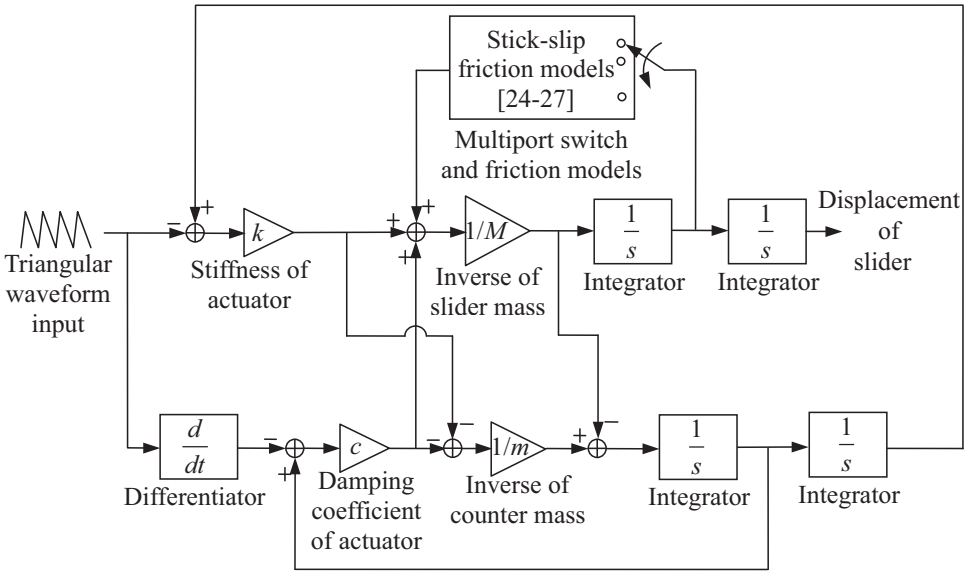

Fig. 8. Functional blocks of dynamic model of IDM for simulations.

4.1. Dynamic model analysis

The dynamic response of Eq. (30) can be expressed as follows:

$$X(t) = (M+m)((A_1\sin(\omega_d t + A_2)e^{-\xi\omega_n t} - A_3)(C\dot{\ell} + K\ell) + m(A_4 t^2 + A_3 - A_1\sin(\omega_d t + A_2)e^{-\xi\omega_n t})F_\mu \quad (31)$$

where

$$\ell(kT+\tau) = \begin{cases} 0 & k < 0 \\ \dfrac{\tau}{\gamma T}S & \text{when } 0 \le \tau < \gamma T \\ \dfrac{T-\tau}{(1-\gamma)T}S & \gamma T \le \tau < T \end{cases}$$

$$A_1 = \frac{m}{K(M+m)}\sqrt{\left(\frac{C}{2M\omega_d}\right)^2 + \left(\frac{m}{M+m}\right)^2}$$

$$A_2 = \tan^{-1}\left(\frac{2Mm\omega_d}{C(M+m)}\right)$$

$$A_3 = \frac{m^2}{K(M+m)^2}$$

$$A_4 = \frac{1}{2m(M+m)}$$

$$\omega_n = \sqrt{\frac{K(M+m)}{Mm}}$$

$$\xi = \frac{C}{2}\sqrt{\frac{M+m}{KMm}}$$

$$\omega_d = \omega_n\sqrt{1-\xi^2}$$

Dynamic analysis can also be performed by implementing SIMULINK software, which involves use of the functional blocks, as shown in Fig. 8. The functional blocks carry out the differential equations of the dynamic model in Eq. (30) solving by the Runge–Kutta method. Simulation results of the dynamic model using parameters listed in Table 1 are discussed after identifying system parameters experimentally.

4.2. Identification of dynamic system parameters

Parameters of the dynamic model must be estimated from the experimentally measured data to forecast the behavior of the mechanism precisely. As mentioned earlier, the dynamic model of IDM with a linearization MCK system consists of a friction model and a linear actuator. The estimated parameters include stiffness K and damping coefficient C of the piezoelectric actuator. To identify these two parameters of the piezoelectric actuator, the slider of the MCK model must be fixed like a level suspension without contacting the friction surface to reduce the complexity of identification. For consistency of the identification, the retraction and the extension of IDM excited by triangular waveform signals are used to feed as the inputs of identification which the hysteresis effect reveals. The dynamics of the mechanism are discrete based on a finite difference approximation to the MCK system. The discrete system of a particular sampling time T_s is specified as follows

$$m(x_i - 2x_{i-1} + x_{i-2}) + CT_s(x_i - x_{i-1} - \ell_i + \ell_{i-1}) + KT_s{}^2(x_i - \ell_i) = 0 \quad (32)$$

The above equation can rewrite as follows:

$$\mathbf{HW} - \mathbf{Y} = 0 \quad (33)$$

where

$$\mathbf{H} = \begin{bmatrix} (x_i - x_{i-1} - \ell_i + \ell_{i-1}) & (x_i - \ell_i) \end{bmatrix}$$

$$\mathbf{W} = \begin{bmatrix} \dfrac{C}{m}T_s & \dfrac{K}{m}T_s{}^2 \end{bmatrix}^T$$

and

$$\mathbf{Y} = -(x_i - 2x_{i-1} + x_{i-2})$$

Converging the identified parameters to a range can be ensured based on a weighted recursive least square (WRLS) adaptive algorithm [28] where **W** refers to the matrix that contains the parameters to be estimated. Ultimately, the stiffness and the damping coefficient must be estimated by an iteration of **W**, followed by

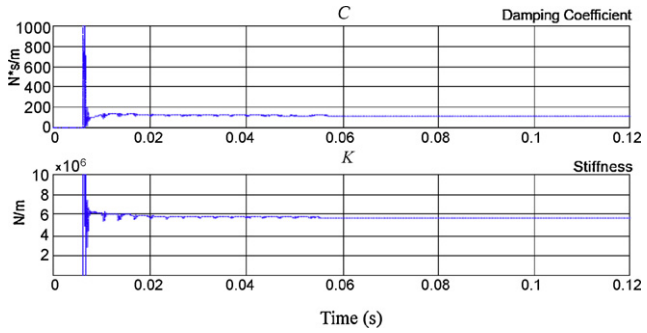

Fig. 9. Experiments for identifying the stiffness K and the damping coefficient C of the MCK system. The identified result of the damping coefficient C is approximately 130 N × s/m and the stiffness K is approximately 5.7×10^6 N/m.

minimizing the value of $||\mathbf{HW} - \mathbf{Y}||$. The optimal solution can be obtained from the following recursive formulation

$$\mathbf{W}_i = \mathbf{W}_{i-1} + \frac{\mathbf{P}_{i-1}\mathbf{H}_i^*}{\lambda_i + \mathbf{H}_i\mathbf{P}_{i-1}\mathbf{H}_i^*}(\mathbf{Y}_i - \mathbf{H}_i\mathbf{W}_{i-1}) \quad (34)$$

where

$$\mathbf{P}_i = \lambda_i \left[\mathbf{P}_{i-1} - \frac{\mathbf{P}_{i-1}\mathbf{H}_i^*\mathbf{H}_i\mathbf{P}_{i-1}}{\lambda_i + \mathbf{H}_i\mathbf{P}_{i-1}\mathbf{H}_i^*}\right]$$

and

$$\mathbf{P}_0 = \mathbf{I}$$

In the evaluation, $\lambda_i = 0.995$ is selected to perform a forgetting factor. Fig. 9 accumulates the parameter estimates identified from the experiments which indicate that the stiffness is approximately 5.7×10^6 N/m and the damping coefficient is approximately 130 N × s/m.

5. Comparison study

Experiments are performing with input frequencies as 100 Hz, 200 Hz, 300 Hz, 400 Hz, 500 Hz, 600 Hz, 700 Hz, 800 Hz and for each input frequency, we set duty ratio as 0.05, 0.1, 0.15, 0.2, 0.25, 0.3, 0.35, 0.4, 0.45, 0.5. For each experimental pair of input frequency and duty ratio, 30 experiments are performed on different sections of the V-groove guide way. The experimental results are shown by either the best representative, committee voting, or the average of all the results. For instance, Fig. 10 displays the experimental results of the representative sets for input frequencies 200 Hz, 400 Hz, 600 Hz, 800 Hz and duty ratio 0.2. In the right of Fig. 10, the symbols from top to bottom represent a multi-step stable case, a one-step stable case, a cut-off case and an illustration of reversed motion, respectively. Reversed motion indicates IDM steps towards the direction of the counter mass as duty ratio of the excitation waveform between 0 and 0.5, which traduces the impulse model incidentally. Movements of the slider of IDM are also clearly observed from the zoom in on the first few steps of Fig. 10. Comparing this figure with Fig. 4(d) reveals that a reversed motion in the impulse model falls to the direction of slider of IDM eventually. In contrast, the dynamic model can derive such reversed motion due to the interaction of a damper and spring. Fig. 11 summarizes the results of the committee voting for each experimental pair (f, γ), i.e. the operating region is determined based on the majority of the behavior of the thirty experiments undertaken during each experimental set; in addition, the experimental results correlate well with the estimated ones. However, some of the one-step stable regions are shaded with multi-step stable symbols, indicating that the impulse model still incurs some of the adverse dynamic effects. These dynamic effects, including the counter mass, oscillate owing to the stiffness and damping coefficient of the piezoelectric actuator, sticktion (stick-slip phenomenon), and hysteresis effect of the piezoelectric actuator [29]. Such effects may cause the slider to oscillate in a high frequency and a high duty ratio region, ultimately failing to comply with the impulse model estimates.

Due to the −3 dB bandwidth of the PZT amplifier used in our experiment, Burleigh PZ-350M is 3 kHz, in which the response on the corner point (velocity discontinuity) of the triangular waveforms is distorted. The impulse spectrum of the velocity discontinuity point, which requires an infinite bandwidth, is clipped at high frequencies in the experiments. The theoretical impulse model

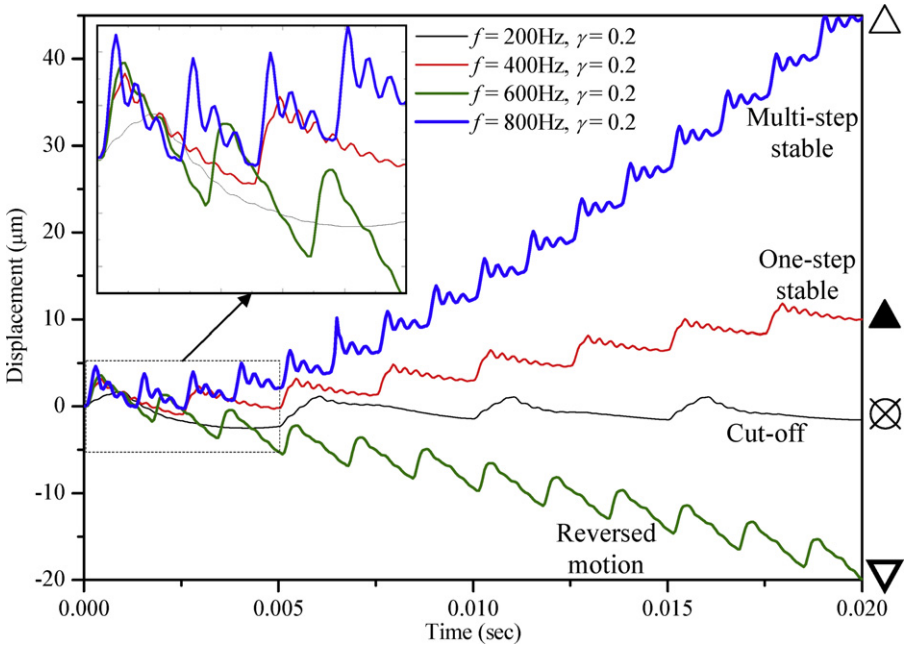

Fig. 10. The experimental results of the representative sets are shown for input frequencies 200 Hz, 400 Hz, 600 Hz, 800 Hz and duty ratio 0.2. The symbols at the right denote the different operating illustrations of IDM.

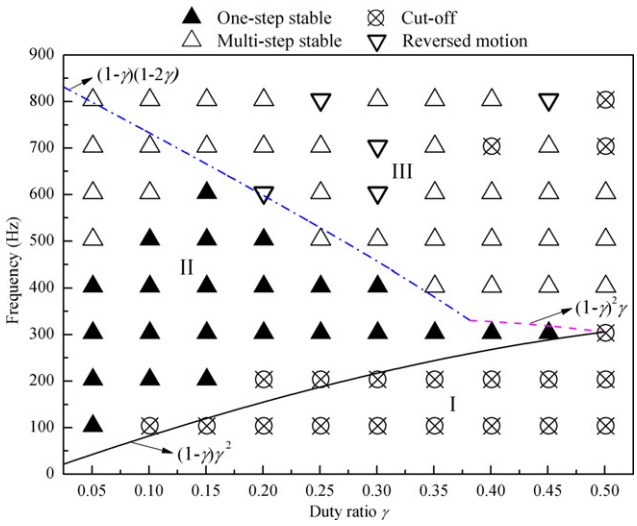

Fig. 11. Experimental results compared with Fig. 4.

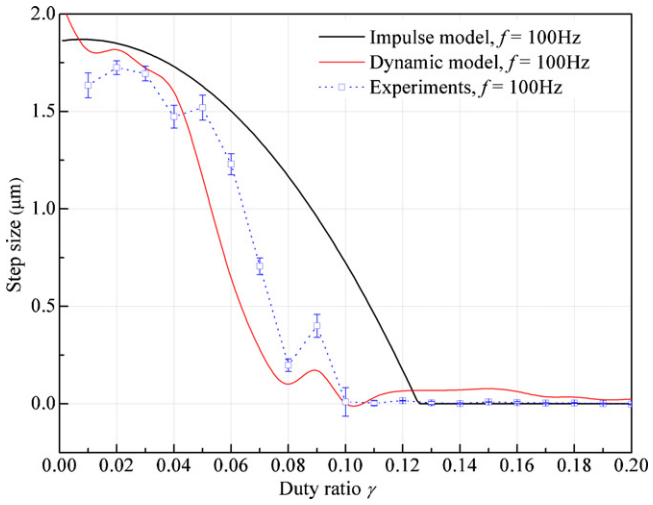

Fig. 12. Comparisons of impulse model (simulation), dynamic model (simulation), and experimental results with excitation input frequency 100 Hz.

and the experimental results more significantly differ at a higher frequency, as shown in Fig. 11.

5.1. Frequency response

Based on Eq. (22) and the system parameters listed in Table 1, the frequency response of the impulse model for the step size is derived, as schematically shown in Fig. 12 with the excitation input frequency 100 Hz and Fig. 13(a) for additional results. In Fig. 13(a), the dashed lines denote the multi-step stable region which each step size is not identical in first few steps. According to these figures, except for the cut-off region, for the same input frequency the step size monotonically decreases with an increasing duty ratio. Except for the cut-off region, for the same duty ratio the step size monotonically increases with an increasing input frequency.

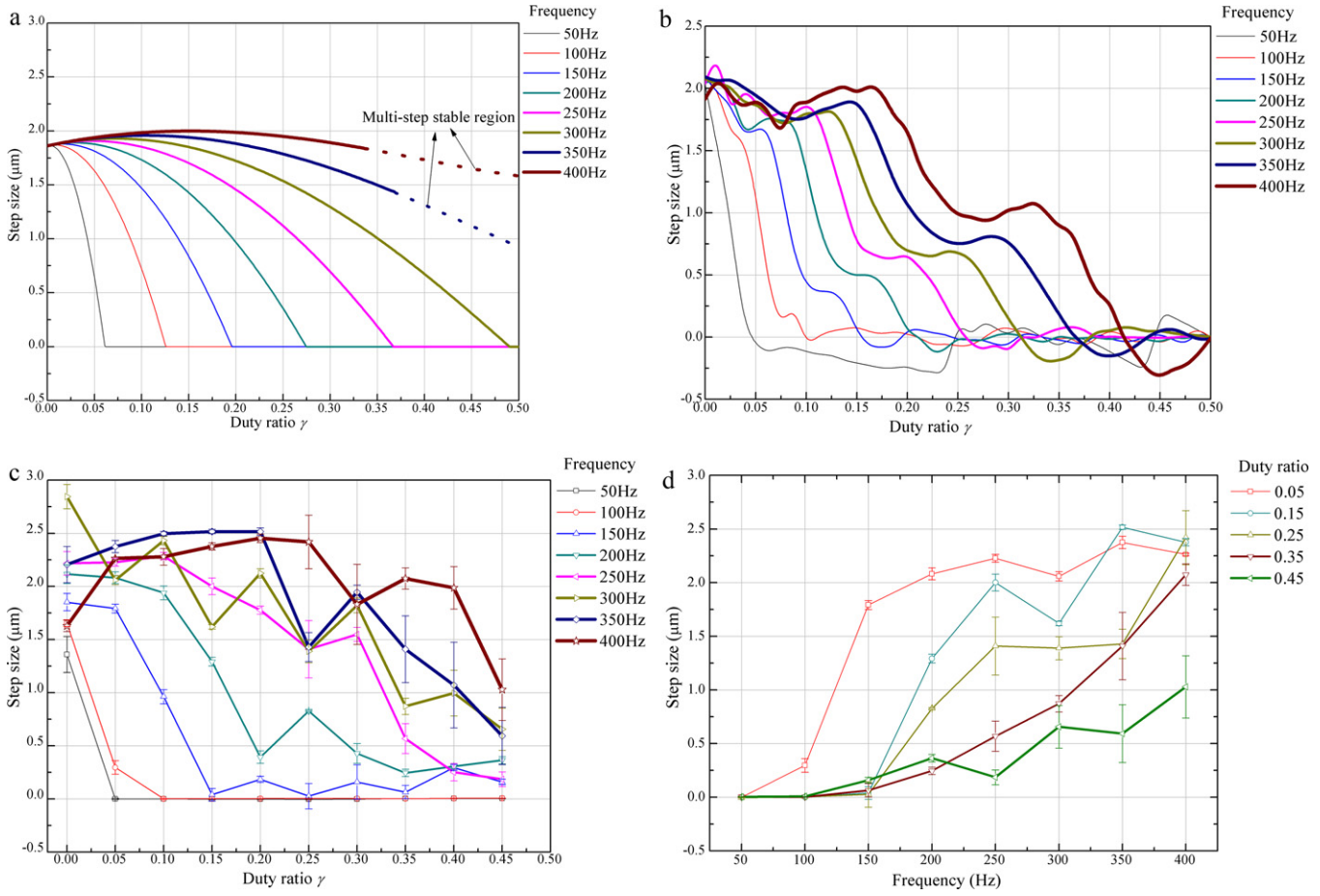

Fig. 13. Step size comparisons: (a) impulse model (simulation), (b) dynamic model (simulation), (c) average of thirty experimental results with respect to different input duty ratio and (d) experimental results with respcet to different input frequency.

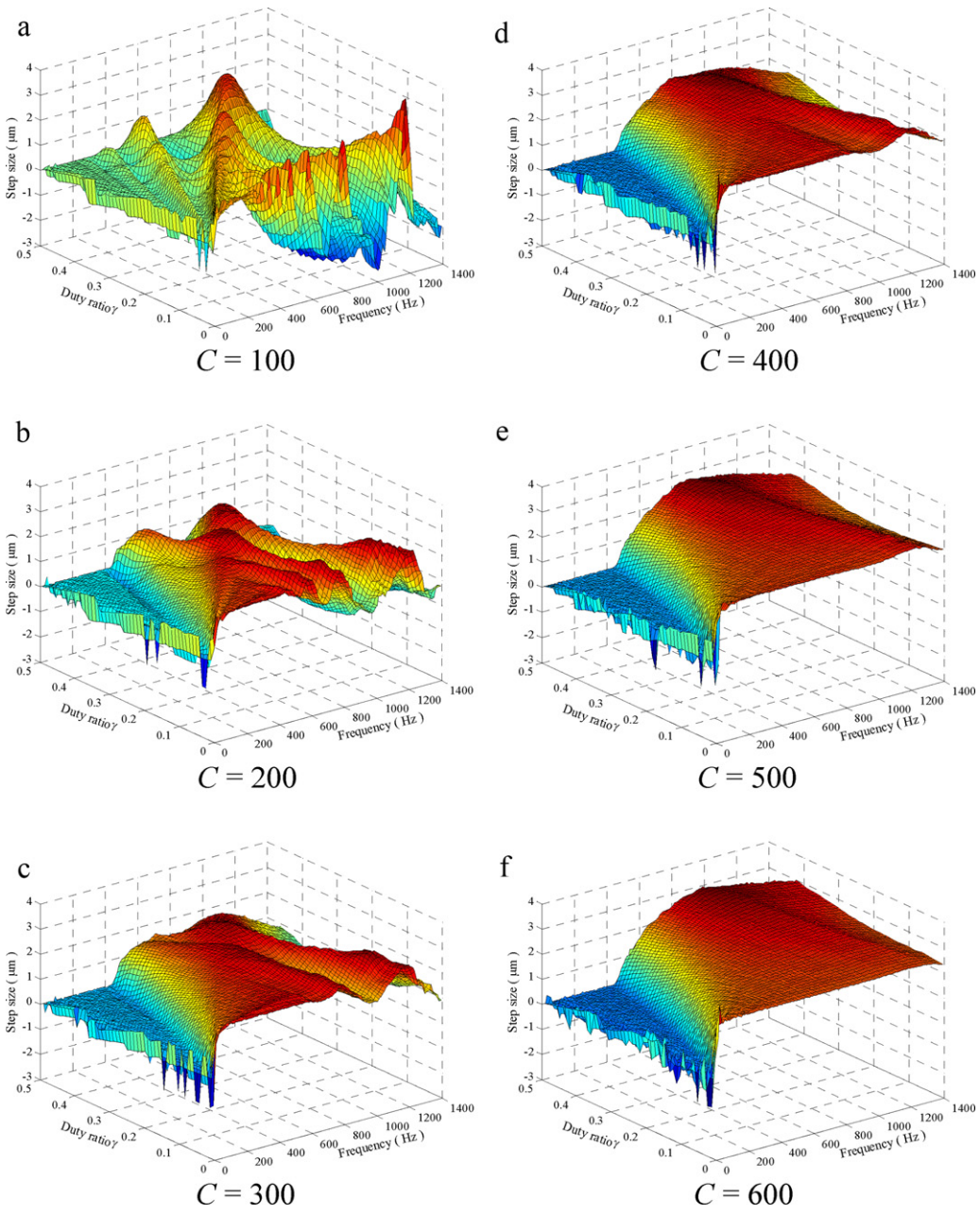

Fig. 14. Effect on step size by changing damping coefficient C with the friction coefficient $\mu = 0.4$ and the stiffness $K = 9 \times 10^6$ N × s/m using dynamic model (simulation).

Based on Eq. (31) and the system identification results, the frequency response of mass–damper–spring dynamic model is simulated, with those results shown in Fig. 12 with the excitation input frequency 100 Hz and Fig. 13(b) for additional results. The dynamic model has a frequency response similar to that of the impulse model in the low input frequency and low duty ratio sets.

Fig. 12 also displays the frequency response of experiments with the excitation input frequency 100 Hz. Fig. 13(c) and (d) shows additional results in terms of input duty ratio and input frequency, respectively. The results are demonstrated based on the average of 30 experiments with variances on the same experimental pair (f, γ). The experiment has a frequency response similar to that of the impulse model in the low input frequency and low duty ratio sets. The experiment has a dynamic frequency behavior similar to that of the dynamic model with an input frequency exceeding 200 Hz. Fig. 12 further indicates that with a satisfactory correlation among the impulse model, dynamic model and the average of 30 experiments with variances, nano-scale positioning can be performed within a duty ratio range from 0.07 to 0.1.

5.2. Dynamic simulation

Determining how system parameters affect the stepping positioning of IDM is rather difficult owing to that the IDM used in the experiments has only a set of system parameters. Alternatively, a dynamic model is simulated to exploit the damping coefficient and the friction coefficient effects. Fig. 14 illustrates the effects due to different damping coefficients C. For the damping coefficient C exceeding 500 N × s/m, the step size tends to decrease monotonically with an increasing duty ratio and, also, increase monotonically with an increasing input frequency. Moreover, the mass–damper–spring model is more appropriate for IDM systems with large damping coefficients, as shown in Figs. 14(d)–(f). Furthermore, the dynamic analysis becomes less sta-

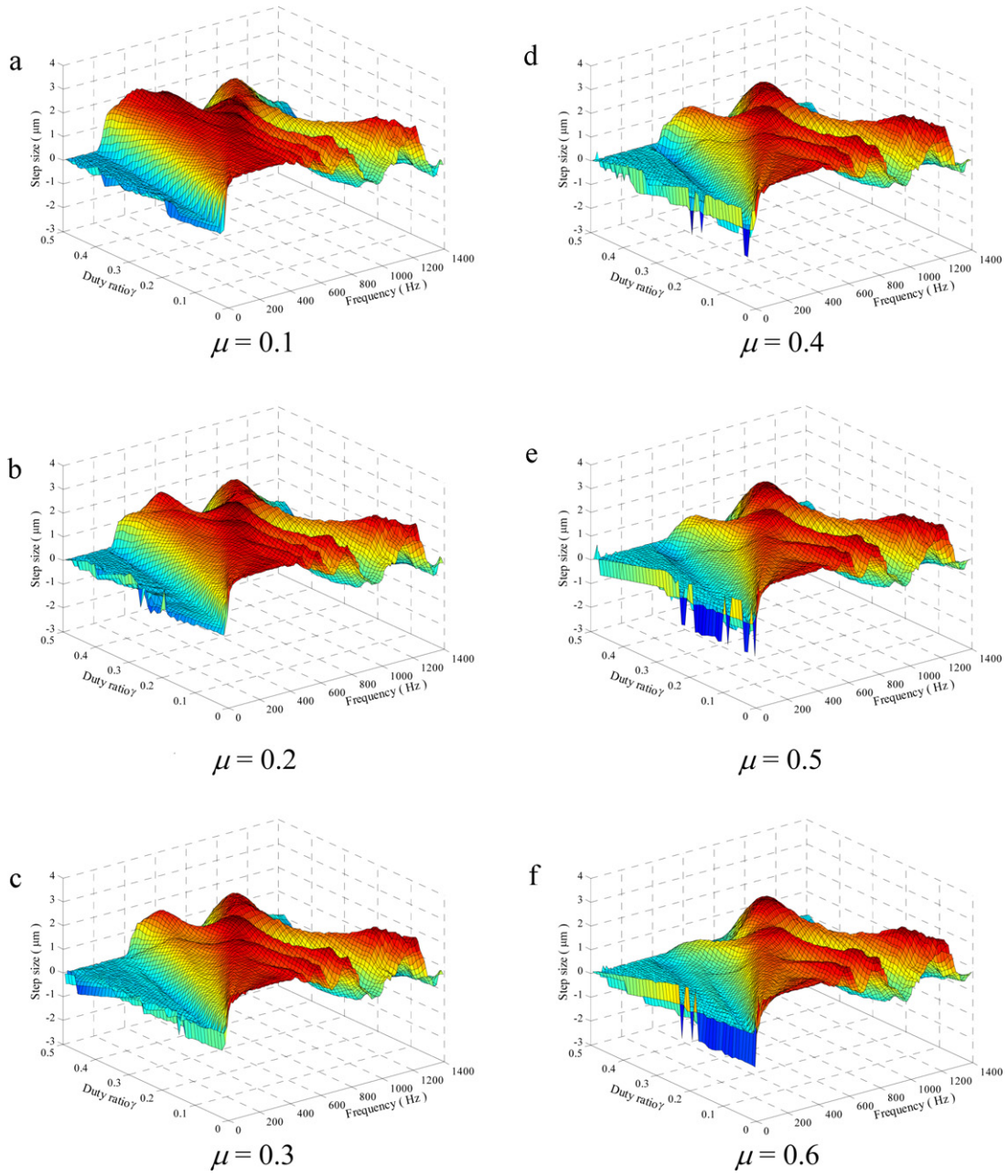

Fig. 15. Effect on step size by changing friction coefficient μ with the damping coefficient $C = 200\ \mathrm{N} \times \mathrm{m/s}$ and the stiffness $K = 9 \times 10^6\ \mathrm{N/m}$ using dynamic model (simulation).

ble for IDM systems with small damping coefficients, as shown in Fig. 14(a)–(c).

Interestingly, the friction coefficient only slightly affects the step size for a small duty ratio and high input frequency. This observation may also be explained from Eq. (21) when

$$\frac{g\gamma^2}{f^2} \ll \frac{m}{(M+m)(1-\gamma)}S \tag{35}$$

the friction coefficient only slightly affects the step size. According to Fig. 15, the coefficient of LuGre friction that is applied in the dynamic model affects the step size to a lesser extent. This observation correlates with experiments reported in the literature [30], which introduced different lubricants to the interface of IDM. Additionally, dynamic model simulated in Fig. 15 complies with experimental results shown in Figs. 11 and 13(c) that has large variances in high duty ratio and input frequency.

6. Conclusion

This work describes two stepping motion models, i.e. impulse model and mass–damper–spring dynamic model, to demonstrate the stepping function of an IDM. The impulse model is applied to classify the operations into a cut-off region, one-step stable region, and multi-step stable region based on different duty ratio γ and input frequency f. In applications requiring accuracy positioning higher than 1 μm, the incremental movement must be achieved exactly in the preliminary phase steps, thus warranting the identification of the one-step stable region for short distance position control. Experimental results indicate that IDM with a proper measurement means can perform the nano-scale in single step precision. During the detailed design phase of IDM, the mass–damper–spring dynamic model can facilitate the designer in forecasting the performance of IDM without fabrication. Therefore, we conclude that the piezoelectric actuators with a higher damping

coefficient yielding similar step sizes due to different input frequencies are preferred in the domain of high precision velocity controls. However, piezoelectric actuators with a lower damping coefficient yielding better correlations between the input frequencies and the duty ratio sets are preferable in the domain of high precision position control. This work provides a significantly contribute of efforts of manufacturers attempting to categorize various applications for different piezoelectric actuators.

Acknowledgements

The authors would like to thank the National Science Council of the Republic of China, Taiwan for financially supporting this research under Contract No. NSC 98-2218-E-009-015 and Mr. Tsai, An-Chen for performing some of the experiments.

References

[1] K. Uchino, Piezoelectric actuators/ultrasonic motors-their developments and markets, in: Proceedings of the Ninth IEEE International Symposium on Applications of Ferroelectrics, ISAF'94, 1994, pp. 319–324.
[2] K Uchino, Piezoelectric ultrasonic motors: overview, Smart Mater. Struct. 7 (1998) 273.
[3] K. Spanner, Survey of the various operating principles of ultrasonic piezomotors, in: Presented at the ACTUATOR 2006, 10th International Conference on New Actuators, Bremen, 2006.
[4] T. Higuchi, Y. Yamagata, K. Furutani, K. Kudoh, Precise positioning mechanism utilizing rapid deformations of piezoelectric elements, in: Micro Electro Mechanical Systems, 1990. Proceedings of an Investigation of Micro Structures, Sensors, Actuators, Machines and Robots, IEEE, Napa Valley, CA, USA, 11–14 February, 1990, pp. 222–226.
[5] J. Mendes, M. Nishimura, K. Tomizawa, Y. Yyamagati, T. Higuchi, Printed board positioning system using impact drive mechanism, in: SICE'96. Proceedings of the 35th SICE Annual Conference. International Session Papers, Tottori, Japan, 24–26 July, 1996, pp. 1123–1128.
[6] K. Furutani, N. Mohri, T. Higuchi, Self-running type electrical discharge machine using impact drive mechanism, in: IEEE/ASME International Conference on Advanced Intelligent Mechatronics'97. Final Program and Abstracts, Tokyo, Japan, 16–20 June (1997) 88.
[7] S.L. Jeng, Y.C. Tung, A multicell linear power amplifier for drivingpiezoelectric loads, IEEE Trans. Ind. Electron. 55 (2008) 3644–3652.
[8] Y.C. Tung, S.L. Jeng, W.H. Chieng, Multi-level balanced isolated floating difference amplifier, IEEE Trans. Circuits-I 55 (2008) 3016–3022.
[9] J.L. Ha, R.F. Fung, C.F. Han, Optimization of an impact drive mechanism based on real-coded genetic algorithm, Sens. Actuators A 121 (2005) 488–493.
[10] Y. Yamagata, T. Higuchi, N. Nakamura, S. Hamamura, A micro mobile mechanism using thermal expansion and its theoretical analysis. A comparison with impact drive mechanism using piezoelectric elements, in: Proceedings of the IEEE Workshop on Micro Electro Mechanical Systems, 1994, MEMS'94, Oiso, Japan, 25–28 January (1994) 142–147.
[11] O. Ohmichi, Y. Yamagata, T. Higuchi, Micro impact drive mechanisms using optically excited thermal expansion, J. Microelectromech. Syst. 6 (1997) 200–207.
[12] R.F. Fung, C.F. Han, J.L. Ha, Dynamic responses of the impact drive mechanism modeled by the distributed parameter system, Appl. Math. Model. 32 (2008) 1734–1743.
[13] T. Ueno, T. Higuchi, Miniature magnetostrictive linear actuator based on smooth impact drive mechanism, Int. J. Appl. Electrom. 28 (2008) 135–141.
[14] T. Ueno, T. Higuchi, C. Saito, N. Imaizumi, M. Wun-Fogle, Micromagnetostrictive vibrator using a U-shaped core of iron-gallium alloy (Galfenol), J. Appl. Phys. 103 (7) (2008) E904.
[15] T. Ueno, C. Saito, N. Imaizumi, T. Higuchi, Miniature spherical motor using iron-gallium alloy (Galfenol), Sens. Actuators A 154 (2009) 92–96.
[16] Y.T. Liu, C.H. Lee, R.F. Fung, A pneumatic positioning device coupled with piezoelectric self-moving mechanism, Asian J. Control 6 (2004) 199–207.
[17] Y.-T. Liu, R.-F. Fung, C.-C. Wang, Precision position control using combined piezo-VCM actuators, Precis. Eng. 29 (2005) 411–422.
[18] S.F. Ling, H.J. Du, T.Y. Jiang, Analytical and experimental study on a piezoelectric linear motor, Smart Mater. Struct. 7 (1998) 382–388.
[19] T.Y. Jiang, T.Y. Ng, K.Y. Lam, Optimization of a piezoelectric ceramic actuator, Sens. Actuators A 84 (2000) 81–94.
[20] J.-L. Ha, R.-F. Fung, C.-S. Yang, Hysteresis identification and dynamic responses of the impact drive mechanism, J. Sound Vibrat. 283 (2005) 943–956.
[21] J.J. Tzen, S.L. Jeng, W.H. Chieng, Modeling of piezoelectric actuator for compensation and controller design, Precis. Eng. 27 (2003) 70–86.
[22] Y.T. Liu, C.W. Wang, A self-moving precision positioning stage utilizing impact force of spring-mounted piezoelectric actuator, Sens. Actuators A 102 (2002) 83–92.
[23] Y.T. Liu, T. Higuchi, R.F. Fung, A novel precision positioning table utilizing impact force of spring-mounted piezoelectric actuator. Part II. Theoretical analysis, Precis. Eng. 27 (2003) 22–31.
[24] D. Karnopp, Computer simulation of stick-slip friction in mechanical dynamic systems, J. Dyn. Syst. Meas. Control-Trans. ASME 107 (1985) 100–103.
[25] C. Canudas de Wit, H. Olsson, K.J. Astrom, P. Lischinsky, A new model for control of systems with friction, IEEE Trans. Automat. Control 40 (1995) 419–425.
[26] J. Swevers, F. Al-Bender, C.G. Ganseman, T. Projogo, An integrated friction model structure with improved presliding behavior for accurate friction compensation, IEEE Trans. Automat. Control 45 (2000) 675–686.
[27] K.J. Astrom, C. Canudas de Wit, Revisiting the LuGre friction model stick-slip motion and rate dependence, IEEE Control Syst. Mag. 28 (2008) 101–114.
[28] A.H. Sayed, Fundamentals of Adaptive Filtering, IEEE Press, Wiley–Interscience, New York, 2003.
[29] J.L. Ha, R.F. Fung, C.F. Han, J.R. Chang, Effects of frictional models on the dynamic response of the impact drive mechanism, J. Vib. Acoust. 128 (2006) 88–96.
[30] K. Furutani, T. Higuchi, Y. Yamagata, N. Mohri, Effect of lubrication on impact drive mechanism, Precis. Eng.-J. Am. Soc. Precis. Eng. 22 (1998) 78–86.

Biographies

Chia-Feng Yang was born in Taiwan, in 1979. He received the B.S. degree in Mechanical Engineering and the M.S. degrees with a major in Mechanical Engineering and minor in Communication Engineering from the National Chiao-Tung University, Taiwan, in 2001 and 2004, respectively. Since 2008, he joined the ARadTek Corporation as a System and Software engineer. He is currently working toward the Ph.D. degree in Mechanical Engineering, National Chiao-Tung University, Taiwan. His fields of interest include piezoelectric micro-actuators and microwave imaging sensors.

Shyr-Long Jeng was born in Taiwan, in 1965. He received a Ph.D. in Mechanical Engineering from National Chiao-Tung University, Hsinchu, Taiwan, in 1996. From 1996 to 1998, he joined an electrical motor design company. He was appointed an Assistant Professor in the Department of Automation Engineering at Ta-Hwa Institute of Technology, Taiwan, in 1998. He is currently an Associate Professor. His current research is in the microprocessor based control and applications in power electrics.

Prof. Wei-Hua Chieng was born in Taiwan, in 1959. He received MSs in Electrical and Mechanical Engineering at Columbia University in 1986 and 1987, respectively. He received a Ph.D. in Mechanical Engineering at Columbia University in 1989. He has awarded the IBM manufacturing fellowship in 1988 and 1989. During his time at Columbia University his adviser, Professor David A. Hoeltzel, has brought him into the research in artificial intelligence for mechanical design. His research interests include the PC-based controllers, motion simulators, and mechatronics devices.